UNIVERSITY OF CALIFORNIA SAN DIEGO

Electrochemical CO_2 Reduction by 2,2’ Bipyridine-5,5’-Biscarboxylic Acid Derived-Rhenium Coordination Polyamides.

A thesis submitted in partial satisfaction of the requirements for the degree Master of Science

in

Chemistry

by

Colin Kane Loeb

Committee in charge:

Professor Clifford P. Kubiak, Chair

Professor Seth Cohen

Professor Nathan Romero

2022

The thesis of Colin Kane Loeb is approved, and it is acceptable in quality and form for publication on microfilm and electronically.

University of California San Diego

2022

Table of Contents:

List of Figures:

Acknowledgements:

This work was performed under the auspices of the U.S. Department of Energy by Lawrence Livermore National Laboratory under Contract DE-AC52-07NA27344.

Abstract of the Thesis

Electrochemical CO_2 reduction by 2,2’ bipyridine-5,5’-biscarboxylic acid derived-Rhenium coordination polyamides.

by

Colin Kane Loeb

Masters of Science in Chemistry

University of California San Diego, 2022

Professor Clifford P. Kubiak, Chair

Rhenium coordinating polyamide derived from 2,2’-bipyride-5,5’-biscarboxylic acid and 1,3-benzenedimethanamine were synthesized, analyzed for structure, and prepared into thin films on graphitic electrodes. Polyamides exhibited varying degrees of polymerization and coordination site occupation with rhenium complexes depending on preparation and synthesis conditions. Polymeric films were demonstrated to be an effective way to fabricate heterogeneous rhenium-bipyridine complexes for electrode fabrication. These materials displayed electrochemical activity and overpotentials similar

to other heterogenized catalysts for selective CO_2 reduction with a faradaic efficiency of 82%, 11,865 TON and TOF of 3.3 s^{-1}.

Introduction:

Carbon dioxide accounts for 76% of anthropogenic greenhouse gas emissions[1] and over the past century global CO_2 emissions have increased by 90%[2]. The Intergovernmental Panel on Climate Change (IPCC) has predicted that the global CO_2 level in the atmosphere may reach up to 570 ppm by the year 2100, from an initial 270 ppm for the pre-industrialized era[3]. To avoid the greatest impacts of climate change, we will need to remove our reliance on fossil fuels as a feedstock for energy and materials while simultaneously pursuing many different methods of carbon capture and sequestration. CO_2 reduction to store energy as carbon neutral fuels and to produce materials is an approach that will address both of the main issues in an economy with a wanning fossil fuel reliance.

CO_2 reduction into value-added products can be accomplished through various methods including biochemical[4], photochemical[5, 6] and electrochemical[7-11]. Recent influx of renewable energy gives rise to a large disparity between electricity supply in the middle of the day when renewable solar energy is most abundant, and when demand is relatively low. There has been significant research and investment into technologies to store this energy for use during non-peak energy production times, such as pumped hydroelectric, thermal energy storage, batteries, and others[12]. This would shift the overall balance of produced energy from fossil fuel reliant energy that is produced in the evenings and at night, to more renewable energy mix. Storing energy generated from renewables in the

form of discrete chemicals, such as hydrocarbons or forming gas, has received less commercial and utility investment; however, this method has the potential to produce an array of products, from plastics materials to fuels for energy storage. When relying on petroleum-based feedstocks, the methods to produce materials and fuels release greenhouses gasses and cannot be considered a viable option in the coming decades. CO_2 is a waste product in many industrial processes and therefore it has the highest potential to be converted into value-added products through various pathways[13]. The development carbon sequestering technology as a sink for excess renewable energy has therefore garnered significant research attention. For these reasons, renewable energy driven electrochemical CO_2 reduction couples well with the future energy grid, which will be fossil fuel independent.

The rhenium bipyridine complex is one of the most extensively studied electrocatalysts for selective CO_2 reduction. When doubly reduced to form the active catalyst, the complex has a singlet ground state that has a formal electron distribution of one electron in the p* orbital of the bipyridine and one electron in the d_z^2 orbital of rhenium. This configuration allows the catalyst to more favorably bind to CO_2 rather than H^+, and results in high selectivity towards CO_2 reduction over H^+ reduction. This selectivity is desired for any real application to avoid an expensive product separation method downstream and to optimize energy usage towards desired production. Kubiak et al. have studied the mechanism and kinetics[10], as well as the specific impact of substituents to the bipridne ligand[8] for rhenium biypridne molecular catalysts. Furthermore, Kubiak et al. have studied heterogenized catalysts in which proven molecular catalysts were deposited onto carbon nanotubes and sequentially cast onto graphitic electrodes[11].

These heterogenized catalysts demonstrated a high current density at low overpotential with selectivity of 99% towards CO_2 reduction. Other studies have produced heterogenized catalysts by using a similar molecular catalyst with a bifunctional ligand as linkers in metal-organic-frameworks (MOF)[5]. That investigation produced an active photocatalyst for selective CO_2 reduction and elucidated a geometric approach to inhibit dimerization of Mn(I) complexes that leads to catalyst attrition.

Heterogenized catalysts benefit from simplified product purification and in the case of electrochemistry, heterogenized catalysts on an electrode are localized to the electronic field emanating from the electrode surface. This allows a system to have a low overall concentration of catalyst, while also having a relatively high concentration at the surface, where electrons flowing from the electrode may induce catalysis. Polymer-bound metal catalysts have been previously studied as a means to immobilize transition metal catalysts while maintaining many solution phase characteristics, such as high activity and selectivity[14]. These materials vary in their approach; from transition metal complexes that are adsorbed to the polymeric support through non-specific Metal-ligand-polymer interactions, or approaches in which a pendent group of the polymer is covalently bound to the metal complex as a ligand[15, 16]. The former example has the advantage of being able to recover the transition metal complex through simple extraction, and therefore able to recycle and/or reuse the catalyst or the polymer support. This approach, however, may suffer from metal leaching from the surface during the course of a reaction, therefore attenuating catalyst performance. The latter example of covalent interactions with π-conjugated polymers have demonstrated electrical and optical properties[17].

Polyamides utilizing 2,2'-bipyridine-5,5'-biscarboxylic acid as a diacid starting material have been previously studied and used in ruthenium-coordinating polymers for their use in single-layer light emitting materials[18]. Similar nitrogen containing groups such as pyridine and imidazolium, have been attached to polymeric backbones, and used to bind transition metal complexes to demonstrate catalytic activity[16].

In this study, we synthesized rhenium coordinating polyamides through two pathways; one in which the polyamide is synthesized from dicarboxylic acid and diamine and later metalated to form the coordination polymer. The second pathway involves synthesizing the rhenium bipyridine complex with carboxylic acid in the 5-position of each pyridine ring. This complex is later polymerized with a diamine to form the coordination polyamide. These two polymers are characterized by NMR and FTIR to discern the structure of the polymer and to study the impact of the individual synthesis pathways. A thin film of the polymer is cast onto graphitic carbon electrodes to make components that are suitable for electrochemical CO_2 reduction. The thin films are characterized by SEM and EDAX to characterize the surface of the electrode and their atomic composition. Coordination polymer electrodes are further characterized with electrochemical experiments including CV and CPE, with which the voltage-dependent current response and catalytic activity are assessed.

Experimental:

Coordinating Polyamide Synthesis:

Chemicals were used as received and were not further purified. Procedure was adapted from literature. A solution of 4% LiCl in hexamethylphosphoramide (HMPA) was made by adding 48 g of HMPA to 2 g LiCl; this mixture was briefly mixed and heated to a homogeneous solution. 0.245 g (1.0 mmol) of 2,2' bipyridine-5,5'-biscarboxylic acid was weighed out into a 100 mL 3-neck round bottom flask. To this, 15 mL of 4% LiCl in HMPA, 3 mL of pyridine, 0.5 mL of triphenylphosphite (TPP), and 0.140 g (1.0 mmol) of 1,3-bis(aminomethyl)benzene were added. **(Figure 1)** The reaction flask was installed under a Dean-Stark trap and an inert nitrogen atmosphere was established. The reaction mixture was heated to 110-120°C with stirring for 24 to 90 hours.

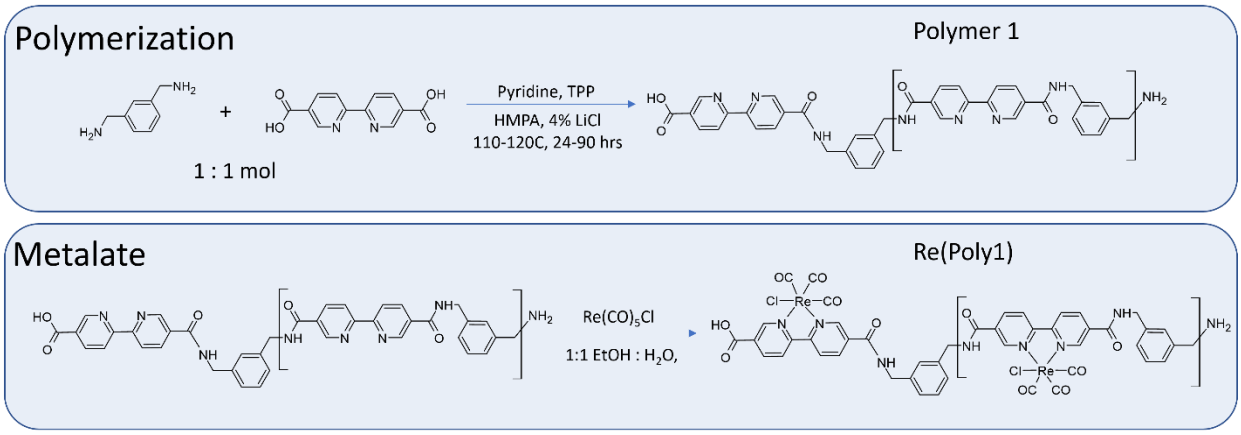

Figure 1: Synthesis scheme 1 in which coordination polyamide are made by first reacting diamine and diacid to produce a polyamide and sequentially metalating the polyamide product

Once the allotted reaction time was complete, the reaction mixture was poured into vigorously stirred room-temperature methanol, creating a white powdery precipitate. This mixture was centrifuged (5000 rpm, 10 min, 10 cm rotor radius) after which the clear supernatant was decanted away, and the precipitate was washed by dispersing into

methanol and centrifuging for 3 cycles followed by 1 cycle using chloroform. The final collected polymer was dried in a vacuum oven at 50C, -90kPa for 24 hours. The final product was a tan solid that presented with an elastomeric character.

0.082 g (0.22 mmol Eq) of Polymer 1, 0.079 g (0.22 mmol) $Re(CO)_5Cl$ were added to a 50 mL round-bottom flask. To this, 25 mL of a 1:1 vol water:ethanol solution was added. The reaction mixture was heated and stirred at reflux for 7 hours. A notable color change from clear to yellow was observed after 20 minutes. During the entirety of the reaction time, dispersed solid polymer could be observed within the reaction vessel. After the allotted reaction time, the mixture was placed under vacuum and solvent was removed. Metalation product was used without further purification.

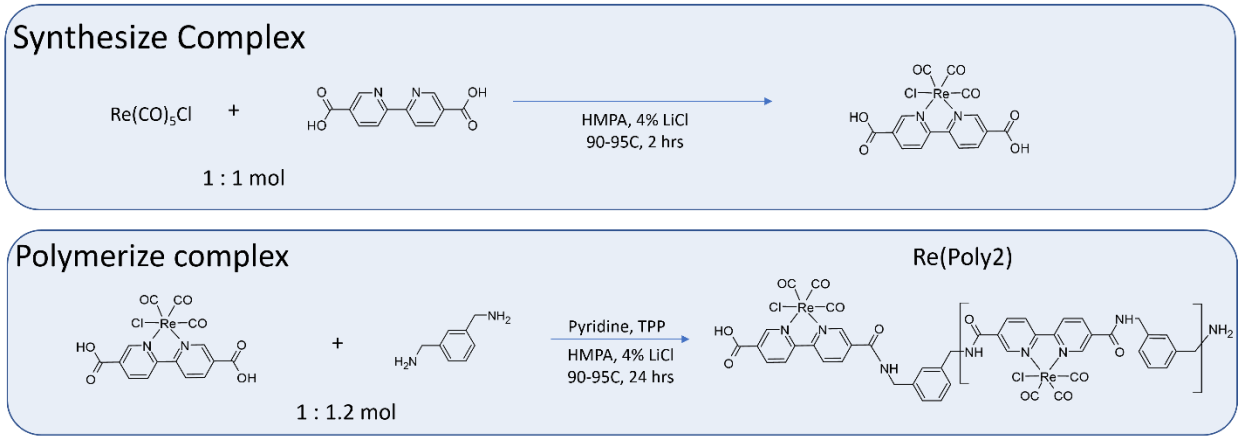

Figure 2: Synthesis scheme 2 in which rhenium bipyridine complex is formed first and sequentially introducing diamine and condensation promoters to synthesize the polymerized coordination polymer.

Following an alternative synthesis method, **(Figure 2)** 0.245g (1.0 mmol) of 2,2' bipyridine-5,5'-biscarboxylic acid and 15mL of 4% LiCl in HMPA were added to a 50 mL 3-neck flask, heated to 90°C and stirred to produce a homogeneous solution. To this, 0.363 g (1.0 mmol) of $Re(CO)_5Cl$ was added and the reaction mixture was held at 90-95°C with stirring for 2 hours. After 2 hours, 3 mL pyridine, 0.5 mL TPP, and 0.215 g (1.5

mmol) of 1,3-bis(aminomethyl)benzene was added to the mixture. After the final addition, the reaction flask was installed under a Dean-Stark trap and the solution was sparged with dry nitrogen. Temperature of 90-95°C was maintained for 24 hours. Polymeric reaction products were separated following the same procedure as above.

Polyamide Characterization:

Dried polymer was cut with a razor blade and characterized by ATR-FTIR, DSC, and TGA. ATR-FTIR was conducted on a Thermo-Fisher Nicolet iS50 Spectrometer equipped with a diamond ATR. Data was collected by 16 scans from 400-4000 cm^{-1} with a resolution of 4 cm^{-1}. DSC sweep was taken from -100°C to 150°C at 2°C /min with a TA instruments 3300 DSC using Tzero pans with hermetically sealed lids.

Electrode Fabrication:

Electrodes were fabricated via drop casting of rhenium coordination polymer from a water:ethanol solution. In a typical preparation, 6 mg of polymer was added to the 1 mL of 1:1 vol. water:ethanol solution, and stirred for 10 minutes prior to casting. This solution was drop cast onto highly ordered pyrolytic carbon (HOPG) or pyrolytic carbon foil (PCF) electrode and dried at 75°C for 8 hours. Prepared electrodes were stored in a desiccator prior to use. For crosslinked polymer films, a 0.1M solution of 1,1,1-Trimethylolpropane triglycidyl ether (Sigma Aldrich) in acetone was prepared. This solution was drop cast in tandem with Re(poly) solution and cured at 75°C for 8 hours.

Electrode characterization:

Electrodes were characterized by SEM, EDAX, Raman, ATR-FTIR and electrochemistry experiments. SEM images and EDAX analysis were conducted on a

Phenom ProX desktop scanning electron microscopy at 15kEv. ATR-FTIR was conducted on a Thermo-Fisher Nicolet iS50 Spectrometer equipped with a diamond ATR. Data was collected by 16 scans from 400-4000 cm^{-1} with a resolution of 4 cm^{-1}. Cyclic voltammetry (CV) and constant potential electrolysis (CPE) experiments were conducted on a BioLogic VSP-300 potentiostat, using the prepared electrode as the working electrode, paired with a pyrolytic carbon foil as counter electrode and Ag/AgCl pseudo reference electrode. Acetonitrile solution containing 0.1M tetrabutylammonium hexafluorophosphate and 5mM ferrocene was used as electrolyte. Acetonitrile was dried over oven-dried 4Å molecular sieves prior to electrolyte preparation and tested by Karl Fisher titration to have a water concentration of less than 50ppm. Prior to electrochemical experiments, solvent-saturated nitrogen or carbon dioxide was sparged through the electrolyte for a minimum of 15 minutes to prime the solution. Electrochemical products from CPE were analyzed by FTIR headspace measurement, in which 100 µL of CPE headspace was injected into a 10 cm path length IR gas cell containing CO_2 minus 100 µL[19]. CO stretch between 2150 cm^{-1} and 2250 cm^{-1} were used to quantify CO produced during CPE. To investigate the impact of a proton donor in the electrolyte on the catalyst performance, electrolyte solution was prepared with 0.1, 0.5 and 1.0M phenol.

Results and Discussion:

Polyamide Synthesis, Scheme 1

A Dean-Stark apparatus was selected for polyamide synthesis to remove water from the reaction vessel and to monitor the extent of the reaction. Condensation of carboxylic acids and amines into amide **(Figure 1)** produces water as a byproduct; the equilibrium of this reaction can be pushed towards the polymeric products by use of a

high boiling point solvent, such as HMPA, and distilling off water during the reaction. Volume of collected water was minimal after 24 hours of reaction time, and much of the volume was adhered to the walls of the condenser. This volume remained relatively unchanged after an additional 66 hours of reaction time. Utilization of pyridine and TPP as a base and condensation promoter, respectively, has been demonstrated to improve yield of diamine and dicarboxylic acid condensation into polyamides[18, 20].

For the non-coordinated polymer (Polymer 1, **Figure 1**) solubility was poor and presents a challenge for initial characterization. This polymer was poorly soluble in polar aprotic solvents such as neat DMSO, acetonitrile, chloroform, tetrahydrofuran, acetone, 2-butanone, ethyl acetate, and butyl acetate. Additionally, the polymer was insoluble in non-polar solvents i.e. C4-C10 alkanes, nor polar protic solvents, neutral water, methanol, ethanol, 2-propanol and 1-butanol. A 1:1 volume solution of ethanol and water had poor solubility; however, this mixture afforded manipulation of the polymer to allow metalation and further processing. Protonation of the polymer in pH = 0 water, or DMSO with HCl proved to solubilize the polymer to form a clear solution and thus allowed detailed characterization by NMR.

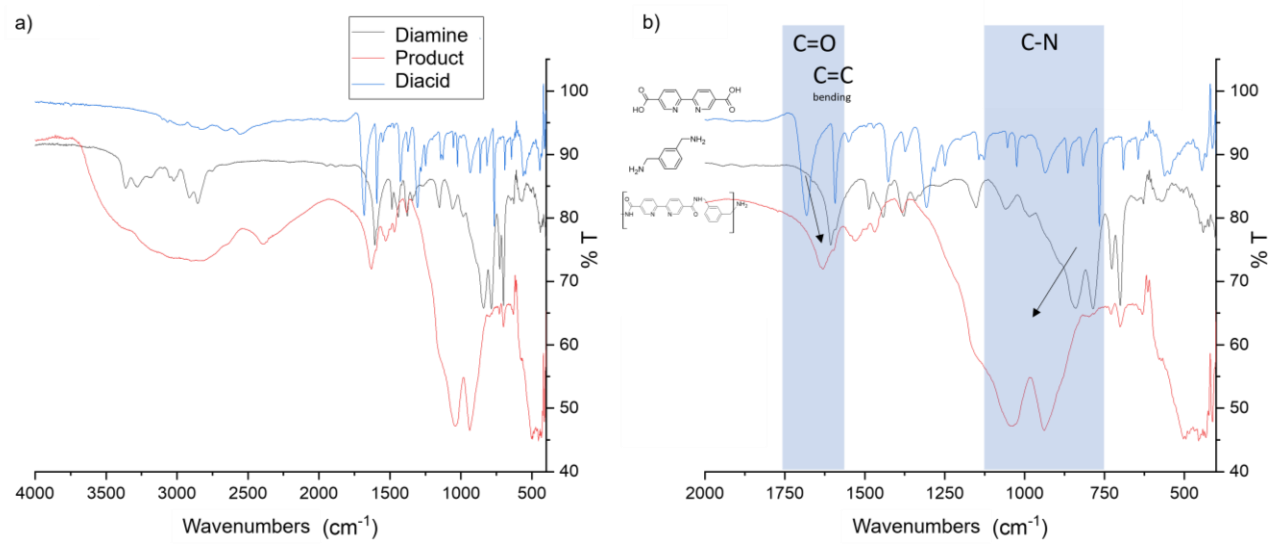

Figure 3: ATR-FTIR spectrum of Polymer 1 product, diacid, and diamine starting material. a) Large O-H band can be observed in the polymeric product indicating hydrogen bonding in the crystaline polymer. b) Carboxylic acid carbonyl stretch (1740cm^{-1}) shifts to lower wave numbers (~1625 cm^{-1}) and carbon-nitrogen stretch (~800 cm^{-1}) shift to higher wavenumbers (~1000 cm^{-1}). This indicates the formation of the benzylic carbon-nitrogen bond of the amide.

ATR-FTIR spectrum of polyamide (Polymer 1), diacid and diamine starting material is presented in **Figure 3**. Carboxylic acid carbonyl peak (1740 cm^{-1}) shifts to lower wave numbers (~1625 cm^{-1}), and carbon-nitrogen peak (~800 cm^{-1}) shifts of higher wavenumbers (~1000 cm^{-1}) from starting material to the product. These shifts in vibrational energies indicate the formation of the benzylic carbon-nitrogen bond of the amide. This suggests the purified product contained the polymerized polyamide presented in **Figure 1**. Large O-H band (3500-2750 cm^{-1}) can be observed in the polymeric product, indicating hydrogen bonding in the crystaline polymer.

NMR of the resulting polymer **(Figure 4)** has similar proton NMR peak patterns from the two starting mateirals **(Figure S1 and S2)**, however there are distict shifts that suggest the polymerized structure. A broad alkyl amine peak that is present in the diamine starting material (**Figure S1**, 3.716 ppm) is missing from the product spectrum, while a broad peak downfield (9.067 ppm) is present; this is indicitave of an amide internal to the

polymer. Peaks related to the bipyridine component (identified by j-coupling values, two doublets, J=7.9 Hz) shifts from 9.2-8.4 ppm in the starting material to 7.6-7.5 ppm in the product. Additionally, peaks are significantly broadened in the product; this suggests a polymeric material, since hydrogen atoms in the chain will have slightly different shielding environments depending on local polymer folding and distance from the chain terminus. This difference in shielding would cause a proton to become diasteriotopic from its monomer equivalent when the proton exists in the polymer. ^{1}H-NMR samples contained impurities that appear on the all spectra presented. Specifically, impurities are partially deuterated DMSO peak at 2.50 ppm, and water introduced with HCl at 3.36 ppm[21].

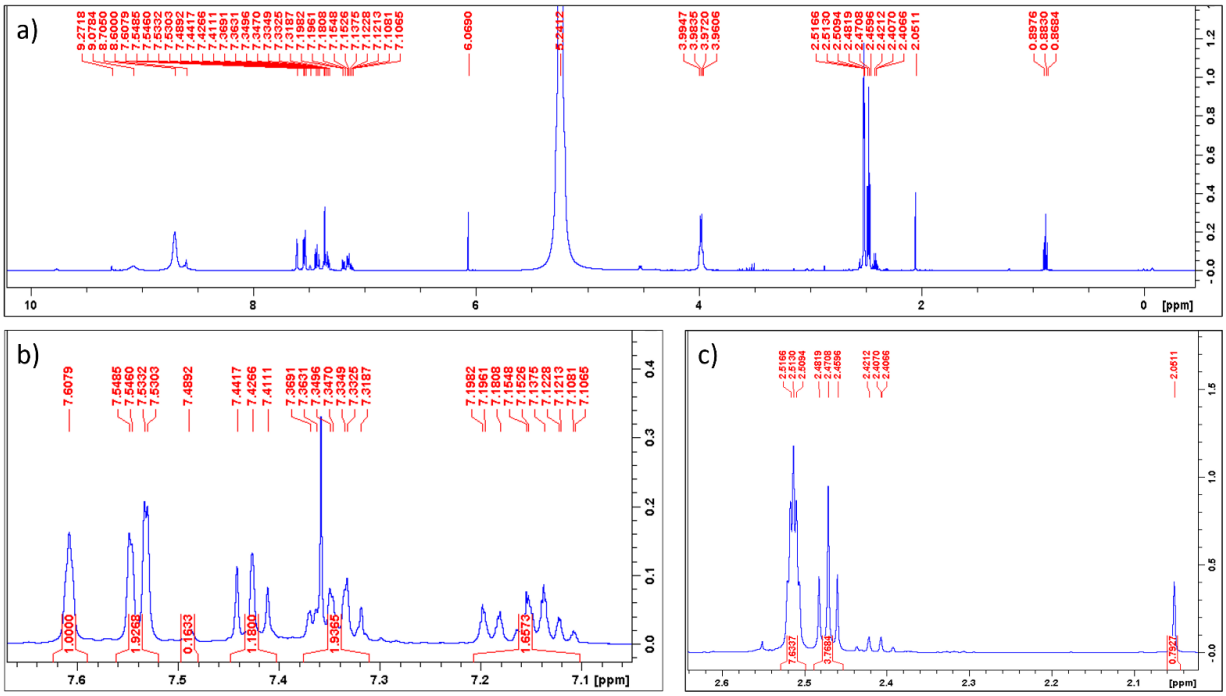

Figure 4: ^{1}H-NMR spectra of Polymer 1 in acidified D_6-DMSO.

DSC of Polymer 1 **(Figure 5)** exhibits a distinct exothermic baseline shift at -46.8°C, slight endothermic baseline shift at c.a. 70°C, and sharp endotherm indicating onset of decomposition at c.a 100°C. This exothermic baseline shift at -46.8°C suggests

a phase shift in the crystallinity of the polymer between two phases which have a different heat capacity. This polyamide is heteroatom rich due to the presence of bipyridine, and has a highly aromatic backbone, therefore, it is expected to have a significant degree of crystallinity from hydrogen bonding and π- π interactions. This shift may indicate a conformational change in the polymer crystallites which lead to a geometric change around the bipyridine or, when metalated, the coordinated-rhenium atom. Exploration of this phase change and its impact on catalysis may present an avenue for future study.

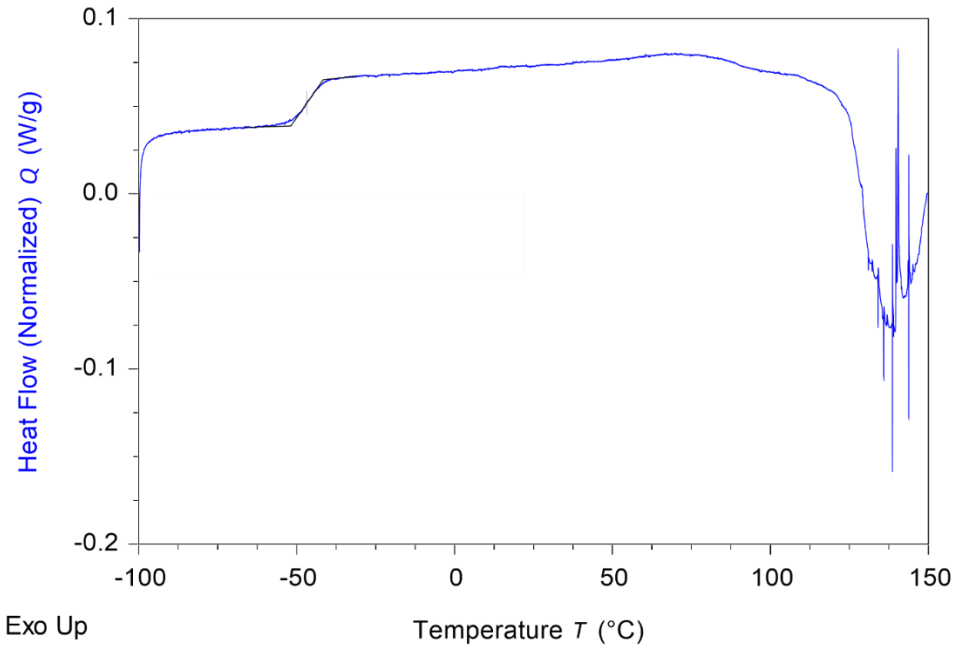

Figure 5: DSC profile of Polymer 1. Polymer 1 sample was heated from -100°C to 150°C. Exothermal base shift at -46.8°C is likely to be a phase shift in the polymer crystal structure.

Polyamide Synthesis, Scheme 2

Synthesis of the initial rhenium complex following **Figure 2** produced a ruby red solution within 40 minutes from the initial tan-yellow color. NMR of the unpurified rhenium complex **(Figure 6, middle)** shows the progression of the reaction by a change in the peak integration at 9.12 ppm. This peak represents the proton in the α-position to the

nitrogen on the bipyridine ring and its integration is dictated by the concentration of unreacted starting material, while the metalated product of this reaction has an α-position proton that is shifted to 9.33 ppm. The ratio of integration between these peaks would yield the fractional extent of the reaction.

Polymerization of rhenium complex was conducted on the unpurified products of metalation. Diamine, pyridine as a base, and TPP as a condensation promoter[20] were added to the reaction mixture, which resulted in a change in color to a light orange color and gradually returned to a ruby red color over 20 hours.

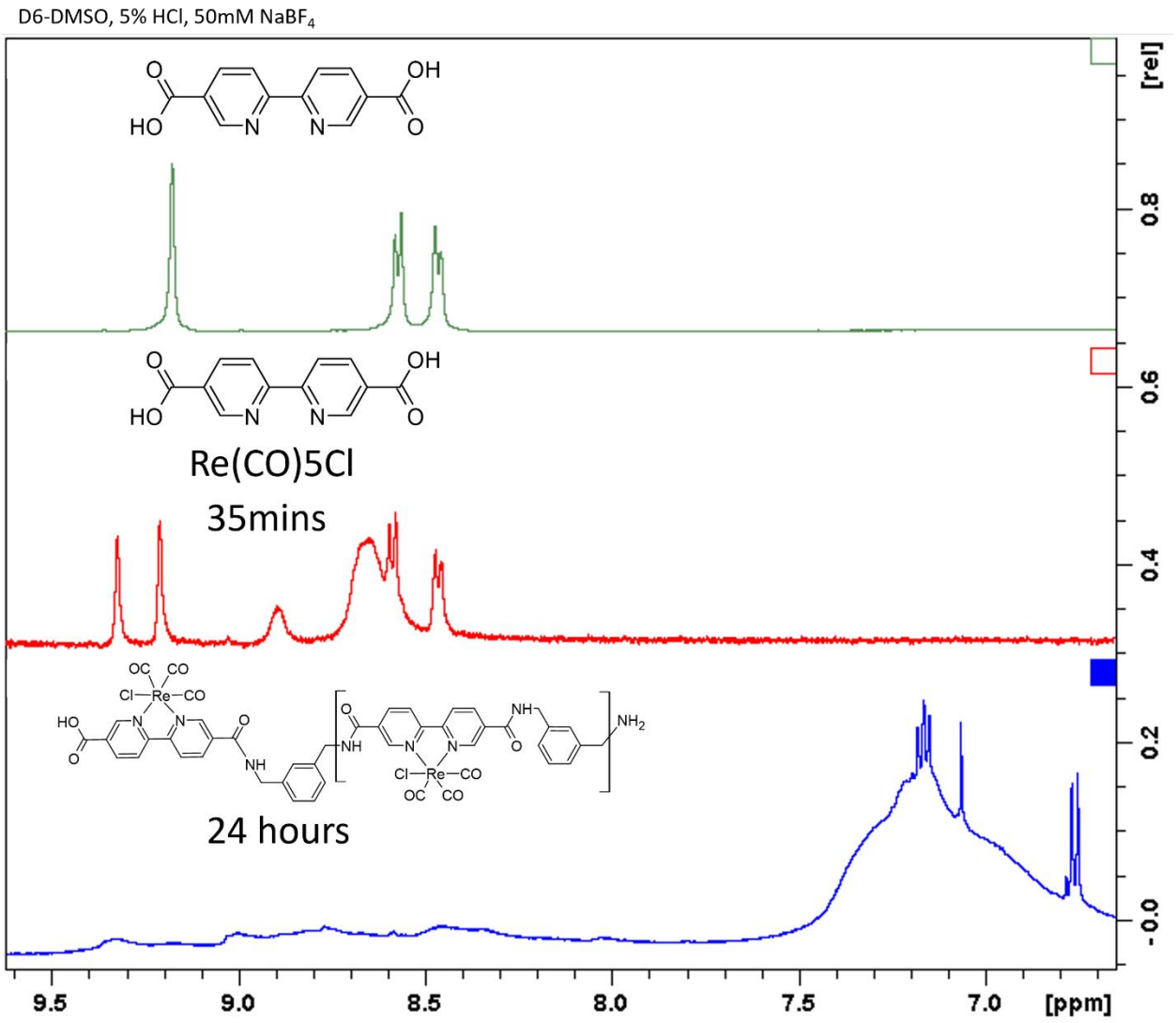

Figure 6: [1]H-NMR Spectra of synthesis timepoints from synthesis Scheme 2. Starting material: 2,2' bipyridine-5,5'-biscarboxylic acid (top). 35 mins into the metalation reaction between 2,2' bipyridine-5,5'-biscarboxylic acid and rhenium pentacarbonyl chloride (middle). Purified polymeric product (Re(Poly2) after 24 hours reaction time (bottom)

Coordination Polymer Characterization:

Purified product from Scheme 2 synthesis was red-orange in color versus the orange-yellow product from Scheme 1 pathway. This obvious difference in color could be indicative of different coordinated metal concentrations in the two materials.

Furthermore, Scheme 2 material was hard but friable, whereas the Scheme 1 material exhibited some elastomeric nature. This may be indicative of the difference in the degree of polymerization between the two materials. Generally, solubility was less of a problem for the metalated polymer compared to the non-coordinating polyamide. This is likely due to stronger solvent interactions with the metal center than the polymer backbone.

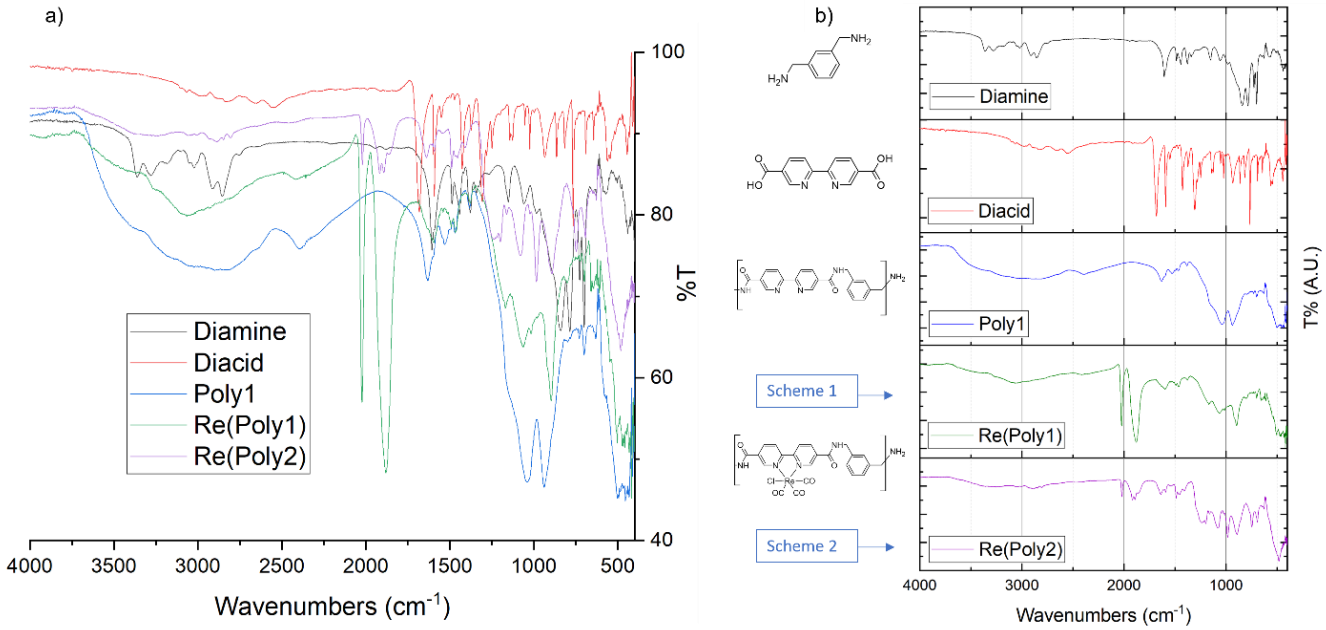

Figure 7: ATR-FTIR spectrum of coordination polymers, uncoordinated polymer, diacid and diamine starting material. Strong distinct stretches at 2020 cm^{-1} and 1874 cm^{-1} are indicative of rhenium carbonyl complexes. Broad O-H stretch (~3750-2500 cm^{-1}), and sharp C=O stretches (~1700-1600 cm^{-1}) suggest the polymeric structure was retained with metalation.

FTIR spectrum of the coordination polymers, intermediate and starting material **(Figure 7)** suggest polymer metalation with rhenium complex and retention of the polymeric structure. Strong CO stretches at 2020 cm^{-1} and 1874 cm^{-1} are indicative of rhenium carbonyl complexes[8]. Additionally, a broad O-H stretch (~3750-2500 cm^{-1}) and sharp C=O stretch (~1700-1600 cm^{-1}) suggest the polyamide structure was retained

with metalation. These vibrational modes correlate to polymeric hydrogen bonding in the heteroatom rich polymer and the C=O stretch of amides that are shifted to lower wavenumbers relative to the carboxylic acid starting material, respectively.

NMR results from the coodinating polymer **(Figure 6, bottom)** are dissimilar to those of the uncoodinated Polymer 1 **(Figure 5)** and rhenium-bipyridine complex **(Figure 6 middle).** Coordination with the metal center at the bipyridine site changes the shielding environment of the bipyridine protons, shifiting the peaks downfield and therefore theroretically allowing calculations of the degree of metalation for the polymer. The coodinated polymer spectrum has a heavily muted spectrum in the range of 9.5 – 7.5 that is indiscernable. Future study is necessiary to purify the coodination polymer and identify an ideal solvent system to obtain a well-resolved spectra.

Fabricated electrode characterization:

Electrodes were fabricated by drop-casting rhenium coordination polymer from an ethanol:water solution. Multiple drops of this solution were applied to pre-cleaned piece of HOPG or PCF and solvent was removed slowly to create a homogeneous film. Electrodes were prepared with coverage areas of approximately 2 cm^2 and contained between 0.5 and 4 mg/cm^2.

Energy dispersive x-ray spectroscopy (EDAX) **(Figure 7)** was mapped onto SEM micrograph **(Figure 15)** of Re(poly)/HOPG electrode. EDAX analysis was conducted across an edge of the Re(poly) film (high contrast) against bare HOPG (low contrast) for comparison. Rhenium and oxygen content was concentrated in the high contrast region of the polymer film, whereas carbon is concentrated in the low contrast region of the bare

HOPG. Signal from carbon is a low energy (ca. 0.2 KeV) peak which indicates low signal density in this region.

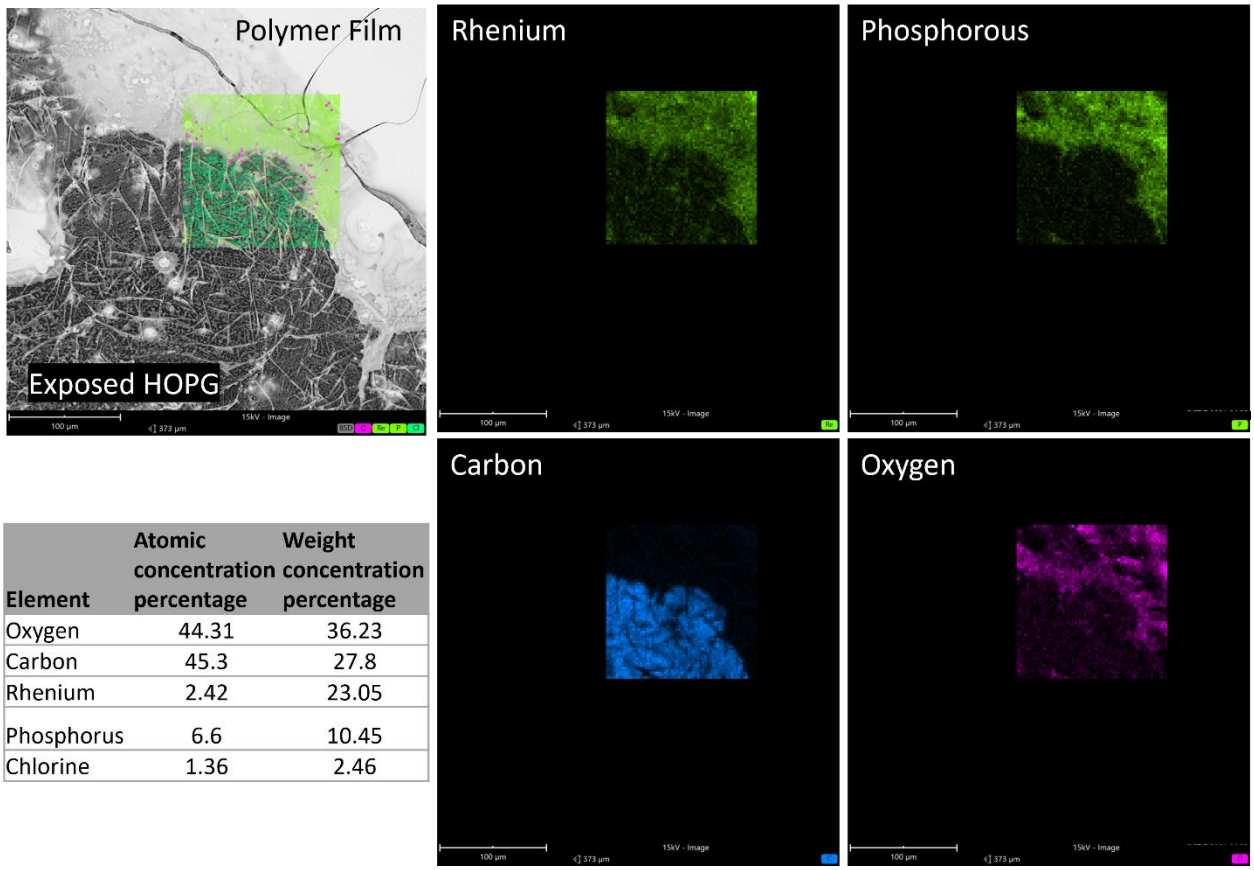

Element	Atomic concentration percentage	Weight concentration percentage
Oxygen	44.31	36.23
Carbon	45.3	27.8
Rhenium	2.42	23.05
Phosphorus	6.6	10.45
Chlorine	1.36	2.46

Figure 8: Energy dispersive x-ray spectroscopy (EDAX) mapping overlaid onto SEM image of Re(poly)/HOPG electrode. EDAX analysis was conducted across an edge of the Re(poly) film (high contrast) against bare HOPG (low contrast). Rhenium and oxygen content was concentrated in the high contrast region of the polymer film, whereas carbon and therefore low signal density is concentrated in the low contrast region of the bare HOPG. EDAX spectral results of phosphorous (2.05 keV) was mapped to the low contrast region, this is expected to be an impurity from electrode fabrication.

EDAX spectral results of phosphorous (2.05 keV) was mapped to the low contrast region of the polymer film, this is in low concentration and is expected to be an impurity from polymer synthesis in the form of HMPA. This high boiling point solvent would be retained from the drying phase and may be involved with polymer swelling. Additionally, EDAX spectral results of phosphorous might be extraneous signal from the HOPG substrate; spot elemental analysis of some regions of the exposed HOPG surface were

measured to have 16.2 atomic % phosphorus. The correlation between EDAX mapped rhenium concentration and observed film location indicate that the rhenium is concentrated within the polymer. Spot elemental analysis of the polyamide film **(Figure 16)** was measured to have between 7 and 14 atomic percent rhenium. Assuming an ideal full occupation of coordination sites within the polyamide, the monomer units would contain 2.0 atomic percent (28.6 wt%) rhenium. The discrepancy between measured value and theoretical value likely has contributions from two main factors[22]: 1) Non-coordinated rhenium ($Re(CO)_5Cl$) or rhenium bipyridine complex could be entrapped in the polymer and therefore inflating the result, or 2) The result for the high-Z rhenium is attributed to the increased sensitivity towards electron excitation and x-ray emission of higher Z elements. Similarly, this effect can be seen from the mapped image of carbon concentration where emissions related to carbon were only mapped on the HOPG regions, and not the slightly-less carbon rich region of the polymer film.

Upon further investigation, scanning electron micrographs of Re(poly)/HOPG electrode **(Figure 15)** reveal structural details of beaded structures within the film and fibrils on the uncoated surface. These structures suggest that a high surface energy environment was involved in depositing the polymer film onto the HOPG substrate. Cracks are apparent on the top surface of the polymer film; this suggests that shrinkage occurred during drying of the drop-cast film. These two surface features have the potential to impact electrode catalytic performance and mass transport of products and reactants; this therefore provides an avenue for future investigations towards catalyst system optimization.

Crosslinked Polymer Film Electrodes:

Crosslinked polymer film electrodes were fabricated by drop-casting a solution of rhenium coordination polymer solution with a crosslinking tri-functional epoxide solution. With the goal to have amine-terminated polyamides, rhenium-coordinating polyamides were synthesized with a 1:1.5 excess of diamine. Amine-terminated polyamides will react rapidly with the epoxide crosslinker and form a crosslinked polymer film that will resist solvation during extended electrochemical experimentation and may improve mechanical properties of the film, lessening the prevalence of cracking on the film. These electrodes withstood electrochemical conditions significantly better than non-crosslinked films which would dissolve away from the electrode surface within an hour. For this reason, crosslinked films were used for all electrochemical experiments.

Electrochemical Experiments:

Cyclic Voltammetry:

Cyclic voltammetry (CV) was used to evaluate the electrochemical response of the coordination polymers. This method varies the potential between the working electrode and reference electrode while observing the resulting current that is passed between the working electrode and counter electrode. Counter and reference electrodes will maintain a similar voltage relative to the working electrode and therefore a plot of current versus potential demonstrates the current dependence on applied voltage. Scan rate is typically held constant for a single scan; however, scan rate may be varied to investigate electrochemical reaction kinetics and whether reactions occur in solution or isolated to the electrode surface.

Rhenium bipyridine tricarbonyl chloride complexes are well-studied electrocatalysts[8-11, 23]. These complexes and their derivatives proceed to catalyze the reduction of CO_2 into CO following the cycle described in **Figure 9**.

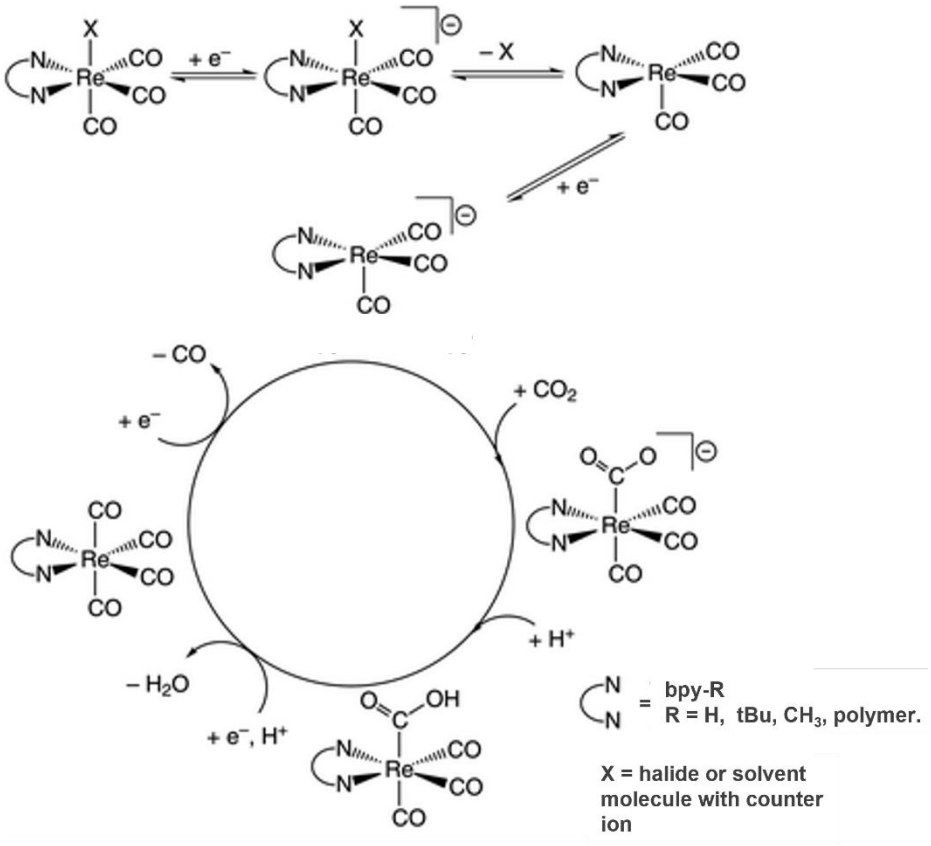

Figure 9: Proposed mechanism of Re(bpy-R)(CO)$_3$Cl with CO_2. Figure adapted from Ref 16b.

On first reduction, the rhenium catalyst undergoes reduction and a ligand-to-metal charge transfer, forming the 6-coordinate anion. With halide dissociate and second reduction the active catalyst is formed. This is a 5-coordinate anion in the top of the catalytic cycle. CO_2 addition and sequential protonation produce the Re^{+1} hydroxy carbonyl species. From this intermediate, there are 2 potential pathways in which CO_2 is reduced: either protonation-first followed by reduction, or reduction-first followed by protonation. Either way, the proton will associate with the hydroxyl group and that group

will leave as water and the electron will satisfy the charge. This will form the rhenium (0) tetracarbonyl species. The last step in the catalytic cycle is a second 1-eletron reduction that results in the dissociation of a carbonyl and regeneration of the active catalyst. Net reaction of CO_2 reduction **(Equation 1)** is a 2-electron process that involves proton donation from a Brønsted acid (HA).

$$CO_{2(sln)} + 2HA_{(sln)} + 2e^- \rightleftharpoons CO_{(sln)} + H_2O_{(sln)} + 2A^-_{(sln)} \qquad \textit{Equation 1}$$

As an electrocatalytic cycle, an applied potential and electric field supply energy for the reaction. Thermodynamic potential of this reaction in acetonitrile ($E^0_{CO_2/CO(MeCN)}$) have been reported to be -0.541 V vs $Fc^{+/0}$. [8, 24] This is the minimum theoretical potential that will drive the conversion of reactants to products. The overpotential is additional potential beyond the theoretical values is needed to further the reaction in experimentally relevant conditions. The additional potential is dependent on experimental conditions, such as solvent and acid concentration.

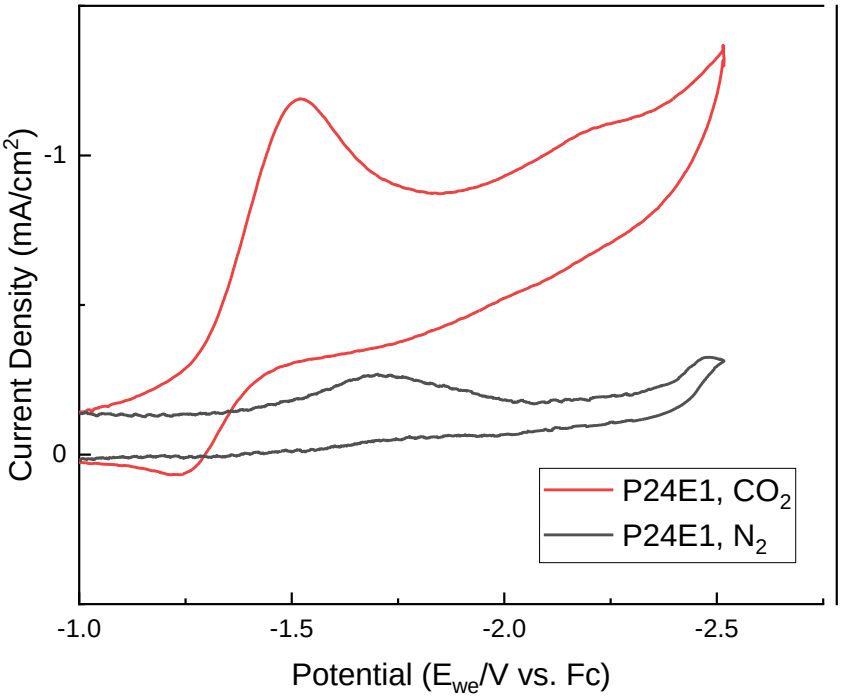

Figure 10: Cyclic voltammogram of Re(poly1) thin film on HOPG electrode with CO_2 (red) and N_2 (black) saturated electrolyte. Electrolyte was 0.1M $TBAPF_6$ in dry acetonitrile, 5mM ferrocene was used as an internal standard. Scan rate was 50mV/s. Full spectrum is in Figure 18

Determination of the catalytic potential, and thus overpotential, is not trivial as experimental results may obscure the catalytic redox couple. There is precedence to use the potential of peak current at half height ($E_{icat/2}$) to estimate the catalytic potential (E_{cat})[25]. CV of Re(poly) thin film on HOPG electrode **(Figure 10)** contains two features that are associated with the coordination polymer film in CO_2 saturated electrolyte. An irreversible redox couple at -1.52V vs Fc and a catalytic current that kicks off at approximately -1.85 V vs Fc and continues for the remainder of the scan window. The irreversible redox feature represents the 1-electron reduction of the rhenium catalyst precursor to the active species. This process is irreversible due to the loss of the halide to the electrolyte, the chloride ion will have a prohibitively low concentration to reassociate with the metal

center. This dissociation is present in CV experiments with CO_2 and N_2 saturated electrolytes since it is not dependent on the catalytic cycle. A slight shift to lower potential with the presence of CO_2 suggests that CO_2 may lower the thermodynamic potential of halide dissociation[9]. The second feature observed in the CV trace represents current that is involved in the catalytic cycle and CO_2 reduction. As suggested previously, the actual E_{cat} of the reaction is not obvious due to the increasing current after 1.85 V. A slight inflection point in the current increase can be observed at -2.220 V vs Fc which was used as a marker for E_{cat} for approximate calculations of overpotential. This results in an overpotential of -1.679 V. This value correlates well to previously studied Re(bpy-R) catalyst in which R is an electron donating group such as tBu, OCH_3 or CH_3[8]. This suggests that conjugated polymer is donating electron density through the amide group to the bipyridine ligand.

Interestingly, we observe only two redox features in CV experiments compared to the three that are expected for the catalytic cycle of Re(bpy-R). For previously studied Re(bpy-R) complexes, features have been observed with better resolution between features. Further investigation is needed to determine what is occurring at each feature. A proposed method to study this is to use TBACl instead of $TBAPF_6$, and to observe the reversibility of the feature at 1.5 V vs Fc. If chloride is dissociating from rhenium when scanning to a more negative potential at -1.5V vs Fc then we would expect to see chloride association when scanning to a more positive potential when the electrode is in an electrolyte that is chloride rich. Spectroelectrochemistry may also be used in the investigation of these redox features.

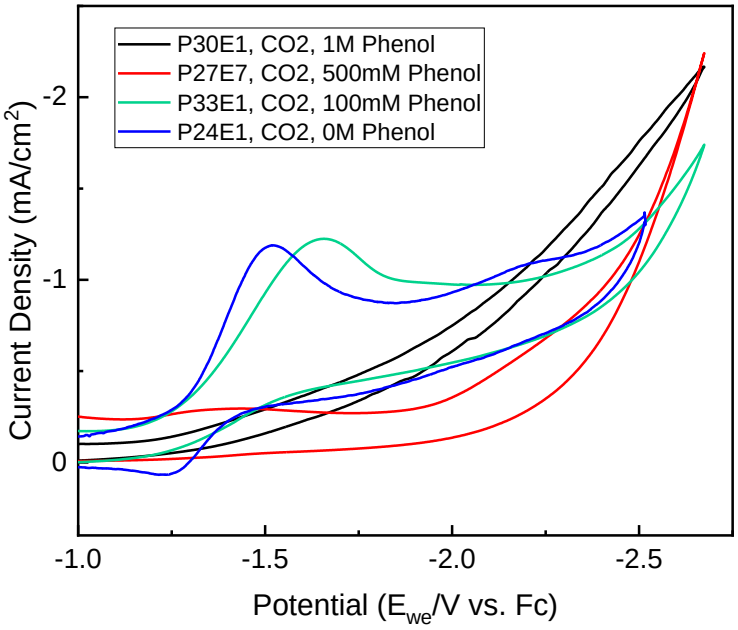

Figure 11: Cyclic voltammogram of Re(poly1) on HOPG with various concentrations of phenol in the electrolyte solution. Electrolyte was 0.1M $TBAPF_6$ in dry acetonitrile, 5mM ferrocene was used as an internal standard. Scan rate was 50mV/s. Full spectrum is in Figure 19

The catalytic cycle of CO_2 reduction to CO **(Figure 9)** requires a proton to be transferred from the bulk to the rhenium carboxylate in order to form the rhenium hydroxyl carbonyl species. It has been previously studied that the introduction of a weak Brønsted acid to the electrolyte solution sufficiently supplies a proton and increases catalytic current. We thus investigated the effect of a weak proton donor on the catalytic behavior on Re(poly). Phenol was selected as a weak proton donor (pKa = 29.1 in MeCN) that would be soluble in our electrolyte and would also not impact the solubility or stability of the polyamide. Electrolytes with various concentrations of phenol were prepared and used with electrodes of similar preparation in CV experiments **(Figure 11)**. It was found that phenol would cause a shift in the catalytic current to more positive potentials while also decreasing current response of couples

associated with halide dissociation. This matches with previous studies in which the current response shifts due to proton donor concentration and acid strength. Furthermore, in the prior study, the presence of a proton donor did not change selectivity for production of CO. For CPE measurements we used phenol as a proton donor at a concentration of 200mM to improve catalyst activity at a moderate overpotential of -1.85V vs Ag/AgCl (c.a. -2.305 V vs Fc).

Constant Potential Electrolysis:

Prepared electrodes were analyzed by controlled potential electrolysis to determine the catalytic performance of rhenium coordinated polymer. For this experiment, electrolyte was saturated with CO_2 and the working electrode was held at a constant potential of -1.85 V vs Ag/AgCl while measuring the current over 60 minutes. **(Figure 12a)** Potential was chosen from previous CV experiments to be a point in which catalytic current was observed. At the end of the experiment, headspace was sampled by gas-phase FTIR to quantify generated CO produced from electrolysis. **(Figure 12b)** Electrolysis current dropped from the initial current to a near steady state value in the first 20 minutes. This response is expected and is attributed to mass transport limitation of reactants to the electrode, specifically the diffusion of CO_2 to the electrode surface is the rate limiting step. Gas-phase FTIR of the headspace shows numerous sharp absorbances in the range of 2050-2220 cm^{-1}. These features indicate the presence of CO in the headspace as a result of electrochemical CO_2 reduction at the Re(poly) centers. This demonstrates the ability of rhenium centers to catalytically reduce CO_2 when coordinating to a polymeric ligand. Total charge transferred was measured to be 3.79 coulombs for the total elapsed time of electrolysis. This yielded 0.39 mL (1.61E-5 mol) of

CO produced. Faradaic efficiency was calculated to 81.9% with a turnover number (TON) of 11,865 and turnover frequency (TOF) of 3.30 s^{-1}.

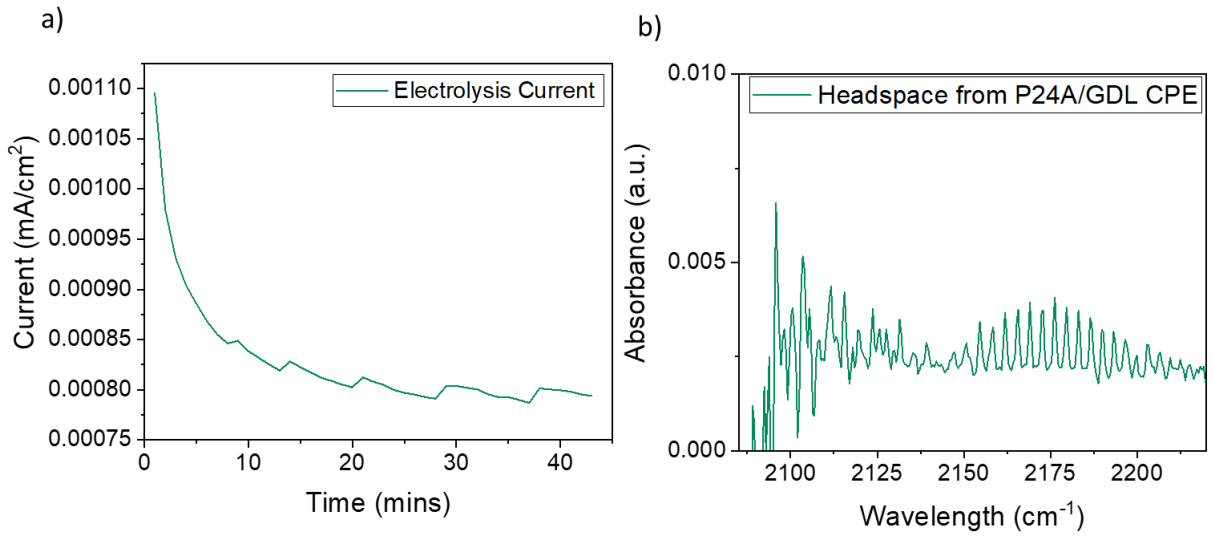

Figure 12: a) Controlled potential electrolysis current over electrolysis time. Electrolyte was 0.1M $TBAPF_6$ and 200mM phenol in dry acetonitrile. b) Gas phase FTIR absorbance spectra of 60 min CPE headspace. The sharp features at 2050-2220 cm^{-1} indicate the presence of CO as an electrochemical product of CO_2 reduction.

Further investigation into the local polymer structure (i.e. polymer folding, hydrogen bonding, crystallinity), and structure-property relationship of the diamine linker are needed to understand the fundamental parameters impacting the catalytic cycle. We present two proposed methods to study the local polymer structure and its impact on the catalytic center. First, we propose synthesizing polyamides with various linker structures (aliphatic, aromatic, bulky, etc.) and comparing the impact on the CV trace. From this we will be able to infer how conjugation and electron density impacts the first bipyridine-based reduction and subsequently redox couples. Second, we propose the use of NOSEY and other 2D NMR methods with various counter ions and proton concentrations to investigate polymer folding and organization. Coupling this work with linker structural investigations may lead to investigations into inhibiting dimerization of

manganese bipyridine complexes that share a similar selectivity towards CO_2 reduction with rhenium complexes.

Conclusion:

Rhenium coordinating polyamides utilizing 2,2'-bipyridine-5,5'-biscarboxylic acid and 1, 3-benzenedimethanamine were synthesized, analyzed for structure, and prepared into thin films on to graphitic electrode. Polyamides displayed properties that suggest varying degrees of polymerization and coordination site occupation with rhenium complexes depending on preparation and synthesis conditions. Polymeric films were demonstrated to be an effective way to fabricate heterogeneous rhenium-bipyridine complexes for electrode fabrication. These materials exhibited electrochemical activity similar to other heterogenized catalysts for selective CO_2 reduction with a faradaic efficiency of 82%, 11,865 TON and TOF of 3.3 s^{-1} at relatively low overpotential. Furthermore, these investigations have revealed the need for future study into the impact of the polymeric ligand on the catalytic cycle. This study presents a novel approach in which to heterogenize molecular catalyst for selective CO_2 reduction. These materials benefit from a macromolecular structure and simple fabrication that may help facilitate commercial adoption and therefore significant carbon sequestration.

References:

(1) Edenhofer, O., R. Pichs-Madruga, Y. Sokona, E. Farahani, S.; Kadner, K. S., A. Adler, I. Baum, S. Brunner, P. Eickemeier, B.; Kriemann, J. S., S. Schlömer, C. von Stechow, T. Zwickel and; Minx, J. C. *Climate Change 2014: Mitigation of Climate Change*. Cambridge University Press, Cambridge, United Kingdom and New York, NY, USA: 2014.

(2) Boden, T. A.; Marland, G.; Andres, R. J. Global, Regional, and National Fossil-Fuel CO2 Emissions. Carbon Dioxide Information Analysis Center, Oak Ridge National Laboratory. *US Department of Energy, Oak Ridge, Tenn., USA 2009. doi 10.3334/CDIAC* **2017**, *1*.

(3) Pieter, T.; E., D. Recent Global CO2 Trend. NOAA/GML: 2021. Masson-Delmotte, V. e. a. *Climate Change 2021: The Physical Science Basis. Contribution of Working Group I to the Sixth Assessment Report of the Intergovernmental Panel on Climate Change*; IPCC, 2021.

(4) Thakur, M.; Sharma, A.; Chandel, M.; Pathania, D. Chapter 9 - Modern applications and current status of green nanotechnology in environmental industry. In *Green Functionalized Nanomaterials for Environmental Applications*, Shanker, U., Hussain, C. M., Rani, M. Eds.; Elsevier, 2022; pp 259-281.

(5) Fei, H.; Sampson, M. D.; Lee, Y.; Kubiak, C. P.; Cohen, S. M. Photocatalytic CO2 Reduction to Formate Using a Mn(I) Molecular Catalyst in a Robust Metal–Organic Framework. *Inorganic Chemistry* **2015**, *54* (14), 6821-6828. DOI: 10.1021/acs.inorgchem.5b00752.

(6) Cheung, P. L.; Kapper, S. C.; Zeng, T.; Thompson, M. E.; Kubiak, C. P. Improving Photocatalysis for the Reduction of CO2 through Non-covalent Supramolecular Assembly. *Journal of the American Chemical Society* **2019**, *141* (38), 14961-14965. DOI: 10.1021/jacs.9b07067.

(7) Jiwanti, P. K.; Sultana, S.; Wicaksono, W. P.; Einaga, Y. Metal modified carbon-based electrode for CO2 electrochemical reduction: A review. *Journal of Electroanalytical Chemistry* **2021**, *898*, 115634. DOI: https://doi.org/10.1016/j.jelechem.2021.115634. Agnew, D. W.; Sampson, M. D.; Moore, C. E.; Rheingold, A. L.; Kubiak, C. P.; Figueroa, J. S. Electrochemical Properties and CO2-Reduction Ability of m-Terphenyl Isocyanide Supported Manganese Tricarbonyl Complexes. *Inorganic Chemistry* **2016**, *55* (23), 12400-12408. DOI: 10.1021/acs.inorgchem.6b02299.

(8) Clark, M. L.; Cheung, P. L.; Lessio, M.; Carter, E. A.; Kubiak, C. P. Kinetic and Mechanistic Effects of Bipyridine (bpy) Substituent, Labile Ligand, and Brønsted Acid on Electrocatalytic CO2 Reduction by Re(bpy) Complexes. *ACS Catalysis* **2018**, *8* (3), 2021-2029. DOI: 10.1021/acscatal.7b03971.

(9) Riplinger, C.; Sampson, M. D.; Ritzmann, A. M.; Kubiak, C. P.; Carter, E. A. Mechanistic Contrasts between Manganese and Rhenium Bipyridine Electrocatalysts for the Reduction of Carbon Dioxide. *Journal of the American Chemical Society* **2014**, *136* (46), 16285-16298. DOI: 10.1021/ja508192y.

(10) Sampson, M. D.; Froehlich, J. D.; Smieja, J. M.; Benson, E. E.; Sharp, I. D.; Kubiak, C. P. Direct observation of the reduction of carbon dioxide by rhenium bipyridine catalysts. *Energy & Environmental Science* **2013**, *6* (12), 3748-3755, 10.1039/C3EE42186D. DOI: 10.1039/C3EE42186D.

(11) Zhanaidarova, A.; Jones, S. C.; Despagnet-Ayoub, E.; Pimentel, B. R.; Kubiak, C. P. Re(tBu-bpy)(CO)3Cl Supported on Multi-Walled Carbon Nanotubes Selectively Reduces CO2 in Water. *Journal of the American Chemical Society* **2019**, *141* (43), 17270-17277. DOI: 10.1021/jacs.9b08445.

(12) *Energy and the Environment - Electricity Storage*. United States Environmental protection Agency, 2022. https://www.epa.gov/energy/electricity-storage (accessed 2022 February 18).

(13) Alok, A.; Shrestha, R.; Ban, S.; Devkota, S.; Uprety, B.; Joshi, R. Technological advances in the transformative utilization of CO2 to value-added products. *Journal of Environmental Chemical Engineering* **2022**, *10* (1), 106922. DOI: https://doi.org/10.1016/j.jece.2021.106922.

(14) Leadbeater, N. E.; Marco, M. Preparation of Polymer-Supported Ligands and Metal Complexes for Use in Catalysis. *Chemical Reviews* **2002**, *102* (10), 3217-3274. DOI: 10.1021/cr010361c. Kobayashi, S. New methodologies for the synthesis of compound libraries. *Chemical Society Reviews* **1999**, *28* (1), 1-15, 10.1039/A707429H. DOI: 10.1039/A707429H. Kobayashi, S. Immobilized catalysts in combinatorial chemistry. *Current Opinion in Chemical Biology* **2000**, *4* (3), 338-345. DOI: https://doi.org/10.1016/S1367-5931(00)00097-1.

(15) Anzenbacher, P.; Král, V.; Jursíková, K.; Günterová, J.; Kasal, A. Porphyrins covalently bound to polystyrene II. an efficient model of monooxygenase reactivity. *Journal of Molecular Catalysis A: Chemical* **1997**, *118* (1), 63-68. DOI: https://doi.org/10.1016/S1381-1169(96)00376-7.

(16) Brunner, H.; Brandl, P. Rh-catalyzed enantioselective hydrosilylation of acetophenone with a polymer-bound pyridine oxazoline. *Z. Naturforsch.* **1992**, *47*, 609 - 613.

(17) Maruyama, T.; Kubota, K.; Yamamoto, T. .pi.-Conjugated soluble poly(6-hexylpyridine-2,5-diyl) and poly(6,6'-dihexyl-2,2'-bipyridine-5,5'-diyl) with high molecular weights and n-type conducting properties. Synthesis, electrical and optical properties, and chemical reactivities of the polymers. *Macromolecules* **1993**, *26* (15), 4055-4057.

DOI: 10.1021/ma00067a052. Wolf, M. O.; Wrighton, M. S. Tunable Electron Density at a Rhenium Carbonyl Complex Coordinated to the Conducting Polymer Poly[5,5'-(2-thienyl)-2,2'-bithiazole]. *Chemistry of Materials* **1994**, *6* (9), 1526-1533. DOI: 10.1021/cm00045a009. Gould, S.; Strouse, G. F.; Meyer, T. J.; Sullivan, B. P. Formation of thin polymeric films by electropolymerization. Reduction of metal complexes containing bromomethyl-substituted derivatives of 2,2'-bipyridine. *Inorganic Chemistry* **1991**, *30* (14), 2942-2949. DOI: 10.1021/ic00014a022.

(18) Yu, S. C.; Hou, S.; Chan, W. K. Synthesis and Properties of Polyamides and Polyesters On the basis of 2,2‘-Bipyridine-5,5‘-Dicarboxylic Acid and the Corresponding Polymer−Ruthenium Complexes. *Macromolecules* **2000**, *33* (9), 3259-3273. DOI: 10.1021/ma991863j.

(19) Esler, M. B.; Griffith, D. W. T.; Wilson, S. R.; Steele, L. P. Precision Trace Gas Analysis by FT-IR Spectroscopy. 1. Simultaneous Analysis of CO2, CH4, N2O, and CO in Air. *Analytical Chemistry* **2000**, *72* (1), 206-215. DOI: 10.1021/ac9905625.

(20) Yamazaki, N.; Matsumoto, M.; Higashi, F. Studies on reactions of the N-phosphonium salts of pyridines. XIV. Wholly aromatic polyamides by the direct polycondensation reaction by using phosphites in the presence of metal salts. *Journal of Polymer Science: Polymer Chemistry Edition* **1975**, *13* (6), 1373-1380, https://doi.org/10.1002/pol.1975.170130609. DOI: https://doi.org/10.1002/pol.1975.170130609 (acccessed 2022/02/15).

(21) Fulmer, G. R.; Miller, A. J. M.; Sherden, N. H.; Gottlieb, H. E.; Nudelman, A.; Stoltz, B. M.; Bercaw, J. E.; Goldberg, K. I. NMR Chemical Shifts of Trace Impurities: Common Laboratory Solvents, Organics, and Gases in Deuterated Solvents Relevant to the Organometallic Chemist. *Organometallics* **2010**, *29* (9), 2176-2179. DOI: 10.1021/om100106e.

(22) Ohring, M. Chapter 10 - Characterization of Thin Films and Surfaces. In *Materials Science of Thin Films (Second Edition)*, Ohring, M. Ed.; Academic Press, 2002; pp 559-640.

(23) Johnson, F. P. A.; George, M. W.; Hartl, F.; Turner, J. J. Electrocatalytic Reduction of CO2 Using the Complexes [Re(bpy)(CO)3L]n (n = +1, L = P(OEt)3, CH3CN; n = 0, L = Cl-, Otf-; bpy = 2,2‘-Bipyridine; Otf- = CF3SO3) as Catalyst Precursors: Infrared Spectroelectrochemical Investigation. *Organometallics* **1996**, *15* (15), 3374-3387. DOI: 10.1021/om960044+.

(24) Azcarate, I.; Costentin, C.; Robert, M.; Savéant, J.-M. Through-Space Charge Interaction Substituent Effects in Molecular Catalysis Leading to the Design of the Most Efficient Catalyst of CO2-to-CO Electrochemical Conversion. *Journal of the American Chemical Society* **2016**, *138* (51), 16639-16644. DOI: 10.1021/jacs.6b07014.
(25) Appel, A. M.; Helm, M. L. Determining the Overpotential for a Molecular Electrocatalyst. *ACS Catalysis* **2014**, *4* (2), 630-633. DOI: 10.1021/cs401013v.

Supporting Information:

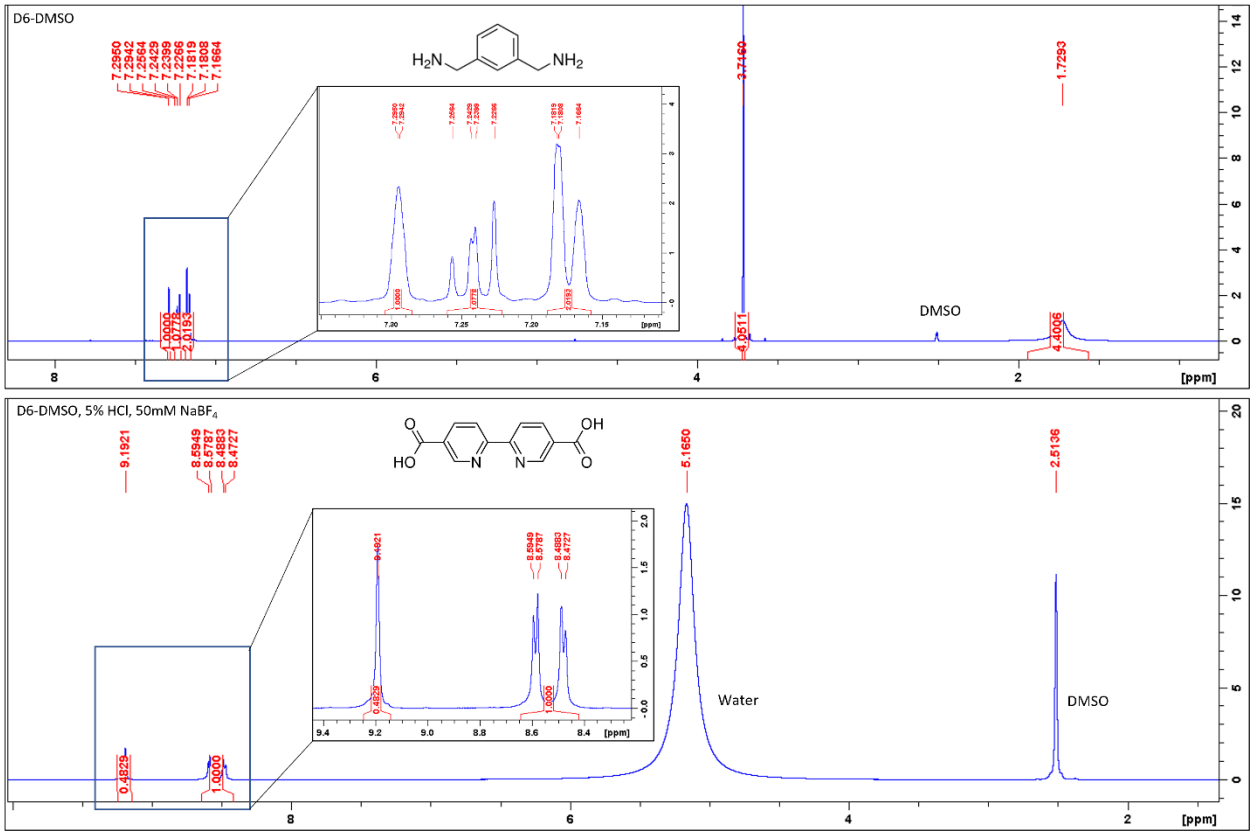

Figure 13: ^{1}H-NMR spectra of starting materials: m-xylylenediamine and 2,2'-bipyridine-5,5'-dicarboxylic acid in D6-DMSO. 2,2'-bipyridine-5,5'-dicarboxylic acid sample contains 50mM $NaBF_4$ and was acidified with HCl to improve solubility.

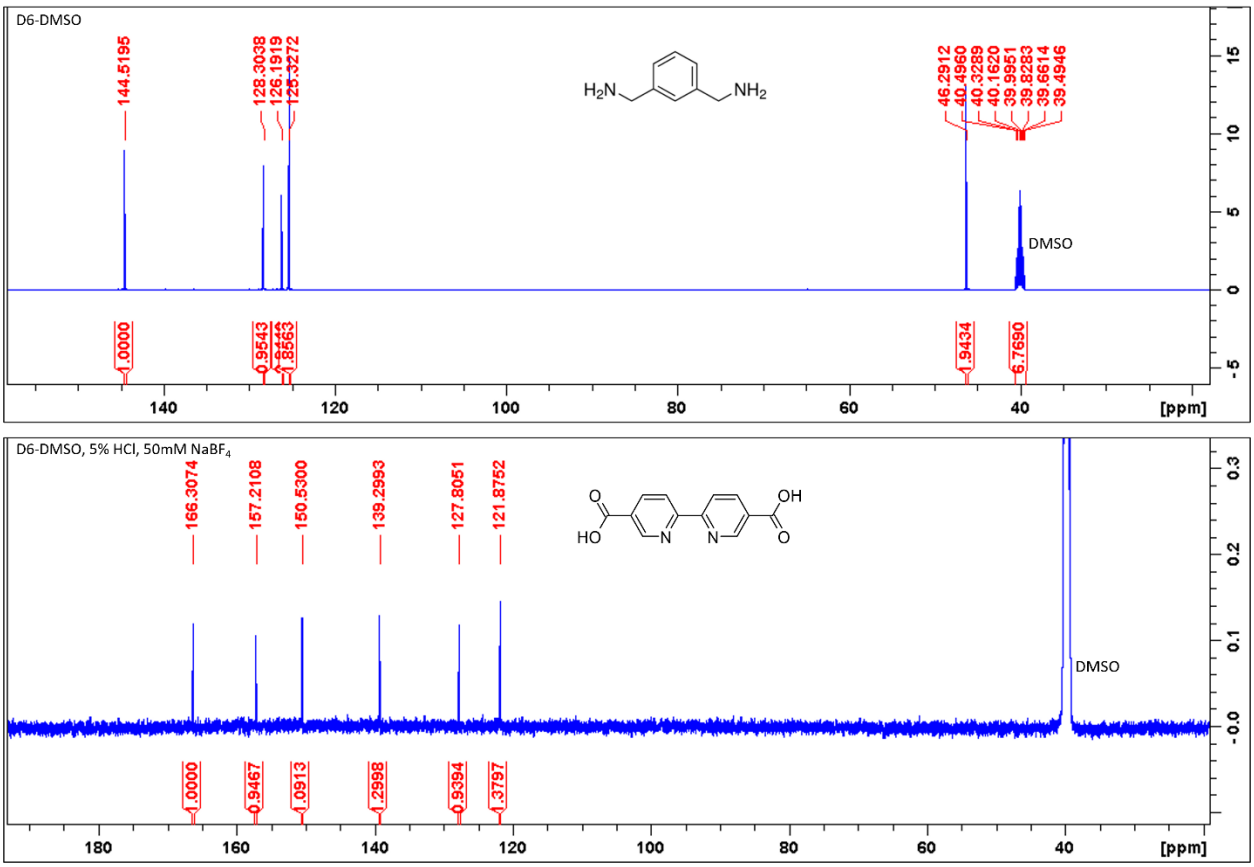

Figure 14: 13C-NMR spectrum of starting materials: m-xylylenediamine and 2,2'-bipyridine-5,5'-dicarboxylic acid in D6-DMSO. 2,2'-bipyridine-5,5'-dicarboxylic acid sample contains 50mM $NaBF_4$ and was acidified with HCl to improve solubility.

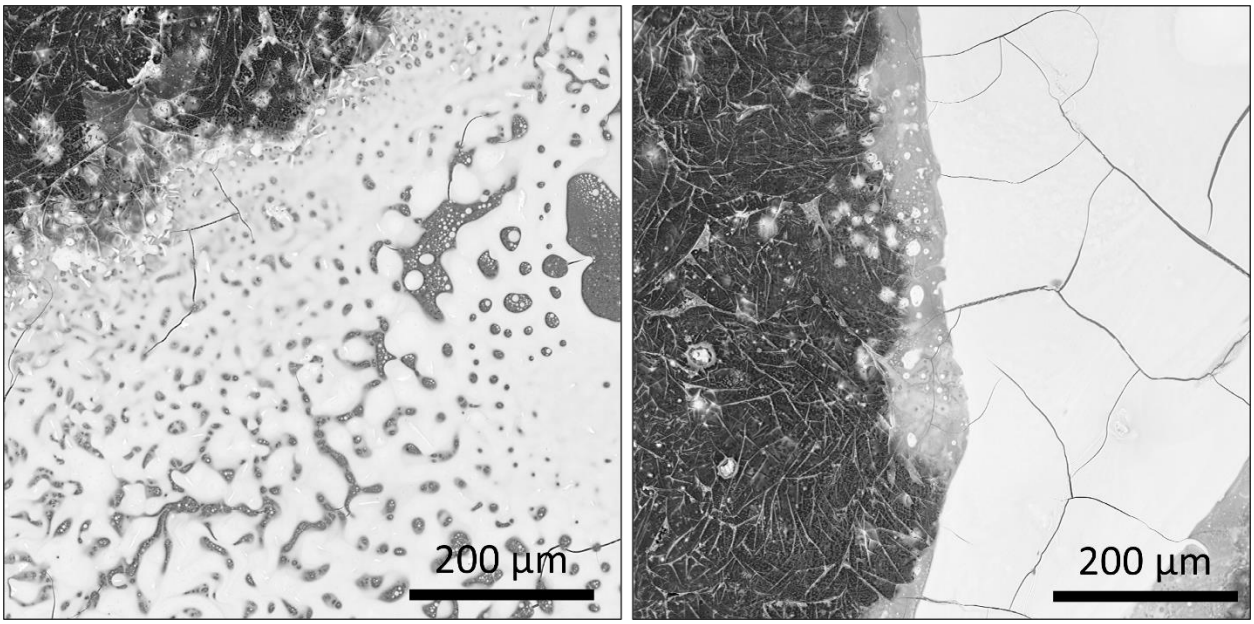

Figure 15: Scanning electron micrographs of Re(poly)/HOPG electrode. Structural details of beaded structures and fibrils suggest a high surface energy environment was involved in depositing the polymer film (high contrast) onto the HOPG (low contrast). Cracks are apparent on the top surface of the polymer film; this suggest that shrinkage occurred during drying of the drop-cast film.

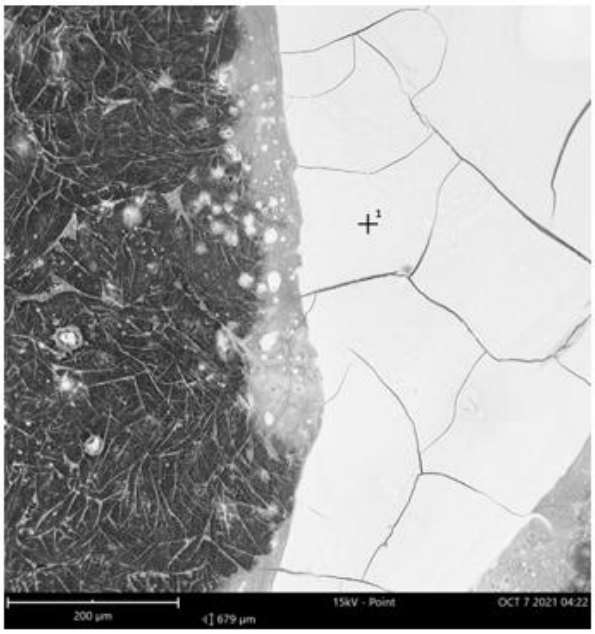

FOV: 679 µm, Mode: 15kV - Point, Detector: BSD Full

Element Number	Element Symbol	Element Name	Atomic Conc.	Weight Conc.
75	Re	Rhenium	7.65	44.54
8	O	Oxygen	64.38	32.20
15	P	Phosphorus	11.21	10.86
17	Cl	Chlorine	4.54	5.03
14	Si	Silicon	5.55	4.87
6	C	Carbon	6.68	2.51

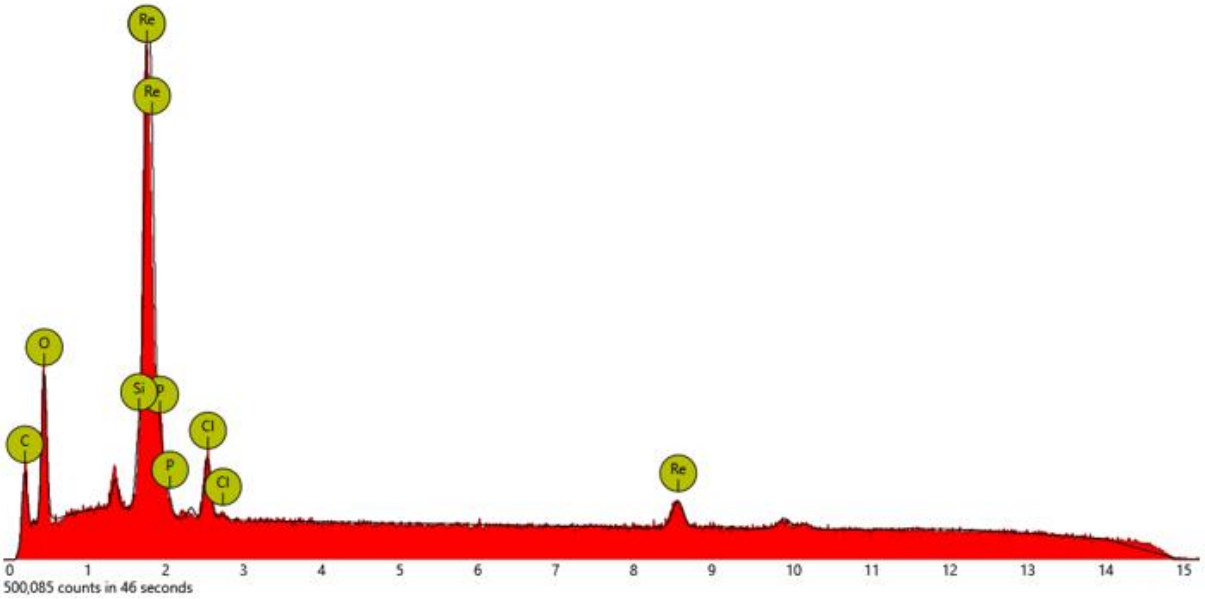

Figure 16: EDAX spot elemental analysis results from a 5x5µm spot area within the polyamide film. P24A on HOPG. Results indicate rhenium concentration is higher than the theoretical ideal coordination polymer film.

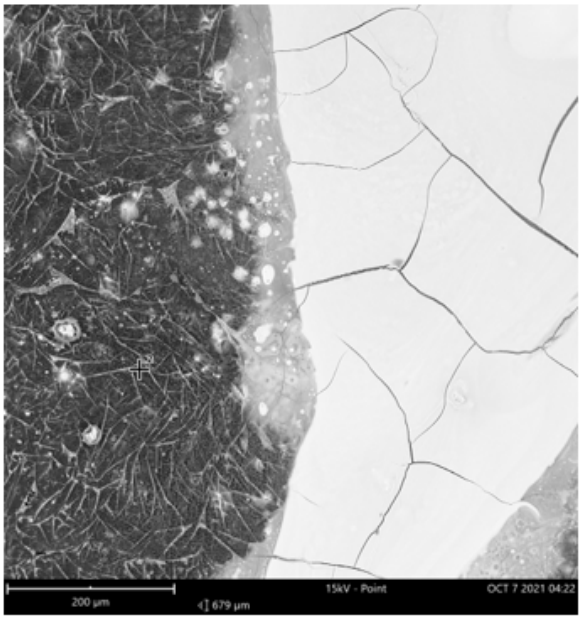

Element Number	Element Symbol	Element Name	Atomic Conc.	Weight Conc.
6	C	Carbon	100.00	100.00

FOV: 679 µm, Mode: 15kV - Point, Detector: BSD Full,

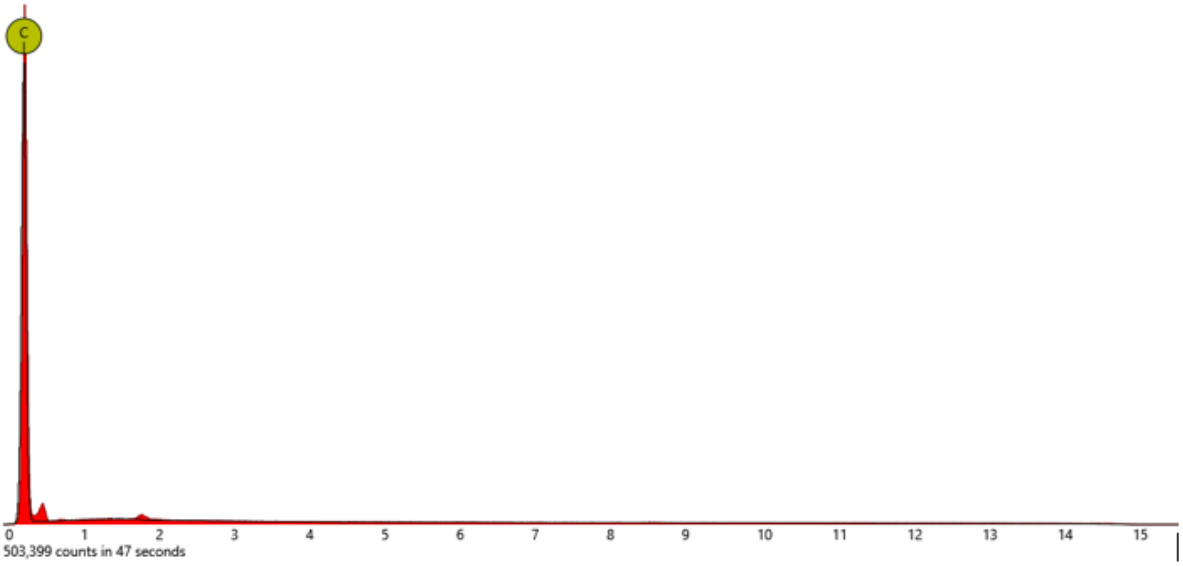

Figure 17: EDAX spot elemental analysis results from a 5x5µm spot area on uncoated HOPG surface. Sample is P24A on HOPG. Results indicate demonstrate the purity of the HOPG substrate.

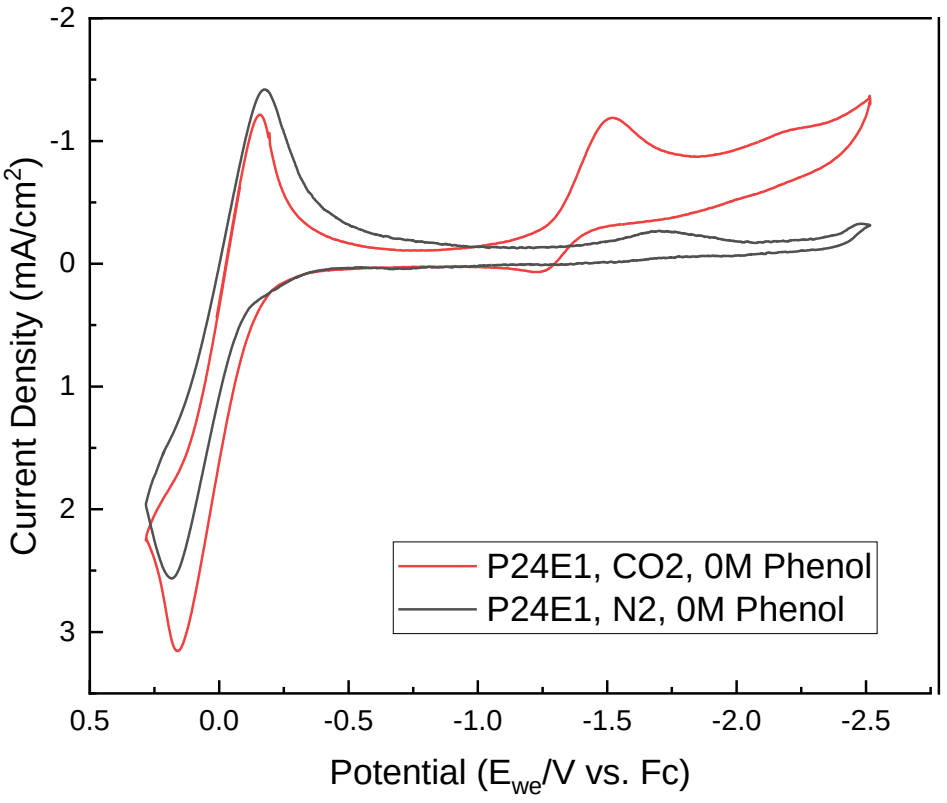

Figure 18: Full CV from CO2 saturated electrolyte versus nitrogen saturated electrolyte study in Figure 10. Redox couple at 0.0V is ferrocene couple used as internal reference.

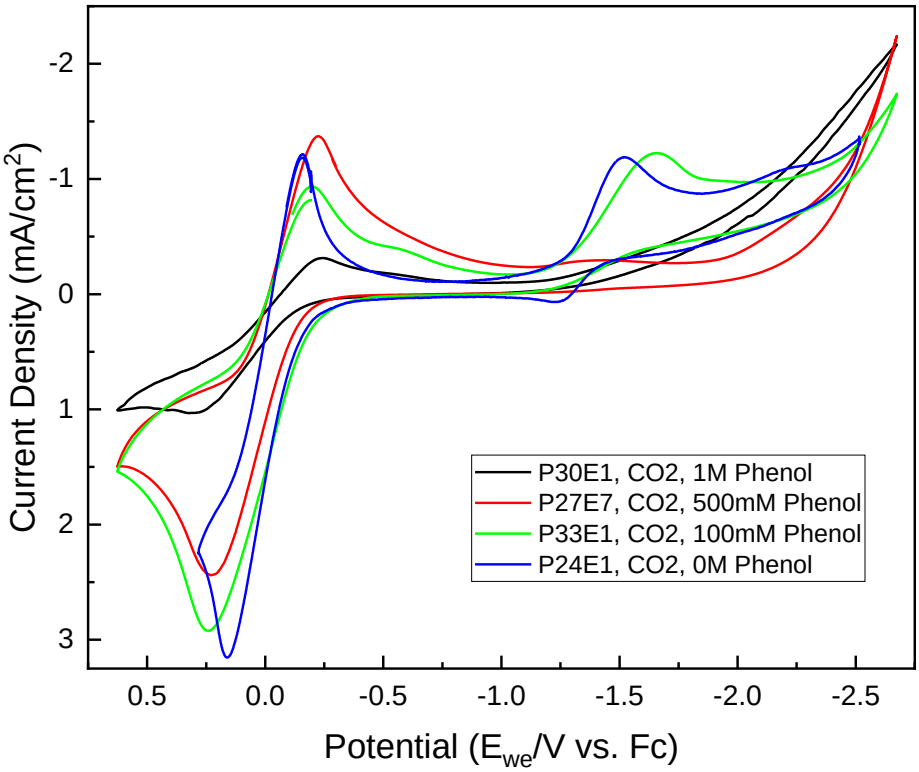

Figure 19: Full CV from phenol as a proton donor concentration study in Figure 11. Redox couple at 0.0V is ferrocene couple used as internal reference.